RSC Advances

ROYAL SOCIETY OF CHEMISTRY

www.rsc.org/advances

1   **Direct delamination of graphite ore into defect-free graphene**

2   **using a biphasic solvent system under pressurized ultrasound**

3

4   H. Beneš[1], R. K. Donato[2], P. Ecorchard[3]*, D. Popelková[1,3], E. Pavlová[1], D. Schelonka[3], O.

5   Pop-Georgievski[1], H. S. Schrekker[2]*, V. Štengl[3]

6

7   *[1]Institute of Macromolecular Chemistry AS CR, v.v.i., Heyrovsky Sq. 2, 16206, Prague 6,*

8   *Czech Republic*

9   *[2]Laboratory of Technological Processes and Catalysis, Institute of Chemistry, Universidade*

10   *Federal do Rio Grande do Sul-UFRGS, Av. Bento Gonçalves 9500, Porto Alegre, RS, Brazil*

11   *[3]Institute of Inorganic Chemistry AS CR, v.v.i., 25068 Řež, Czech Republic*

12

13

14   **Abstract**

15   The study reported herein describes for the first time a method for producing defect-free

16   graphene directly from its mineral ore. This was achieved by treating graphite ore in an ionic

17   liquid containing biphasic solvent system, applying pressurized intense cavitation ultrasound.

18   Without any graphite ore pre-treatment, large few layer thick graphene sheets, as well as

19   micrometric layered crumpled graphene structures, were produced. This opens new

20   opportunities for the development of graphene-based technologies.

21

1 Introduction

2   Since the 1940s, graphene sheets of interconnected sp^2-hybridized carbon atoms have

3 been known.[1] Although this material was considered as "unrealistic" due to its synthetic

4 hurdles and low thermodynamic stability at ambient conditions, Geim and Novoselov

5 changed this perspective in 2004.[2-4] From this point of showing that graphene is a "possible"

6 material with a huge potential for the development of high-tech applications, intensive

7 research efforts have been focused on enhancing its accessibility.

8   Nowadays, few-layers thick graphene nanosheets can be produced by several

9 methods; such as mechanical exfoliation (repeated peeling),[4] solvation force-induced

10 exfoliation,[5] and chemical oxidation/reduction[6-8] of graphite, unrolling of multiwall carbon

11 nanotubes (MWCNT),[9-11] epitaxial growth,[12] chemical vapor deposition (CVD),[13]

12 electrochemical reaction[14] and gas-phase synthesis.[15] Common drawbacks of these techniques

13 are very low yields, high-energy demands and/or necessity to use expensive high-quality

14 substrates. Another important aspect to consider is the quality of the produced graphenes. For

15 instance, the chemical reduction of oxidized graphite is incomplete and produces graphenes

16 with residual functional groups, causing the loss of the inherent graphene properties (*i.e.*

17 electrical, mechanical and thermal properties).[16,17] Therefore, the choice of the proper

18 chemicals and processing conditions is essential for obtaining defect-free graphene

19 nanosheets.

20   Within this context, sonication of graphite has shown to be a powerful tool for the

21 preparation of graphene, although this requires the adjustment of the medium's surface energy

22 close to that of graphene (~ 68 mJ.m^{-2}).[26,27] Besides the medium's surface energy, the strength

23 of the medium-graphene physical interaction is another important parameter. A variety of

24 solvents and solvent combinations that prevent reverse graphene aggregation (e.g. ethylene

25 glycol, dimethylsulfoxide [DMSO], dimethylformamide [DMF], *N*-methyl-pyrrolidone

26 [NMP], c-butyrolactone, dimethylacetamide, or its mixtures with water) have been

27 successfully applied in the exfoliation of graphite under high-intensity ultrasound waves from

28 an ultrasound horn, producing solvated graphene flakes.[18,19] This strategy allows the

29 preparation of graphene monolayer dispersions in DMF,[20,21] benzene[22] and NMP[19,23]. In

30 addition, the medium's surface energy can be adjusted by the addition of a surfactant, which

31 has been achieved with sodium dodecylbenzene sulphonate in a water solution, providing

1   stable graphene suspensions.[24] Despite these advances, the maximum achieved graphene

2   sheets concentrations remain low, around 1 mg/mL.[25]

3   Considering the potential use of surfactants and the importance of the physical

4   medium-graphene interaction, imidazolium ionic liquids (IL) open new opportunities. The π-

5   electron cloud of the imidazolium cation provides relatively strong interactions with various

6   π-electronic carbon nanomaterials, including MWCNT, fullerenes and graphene.[28] Besides the

7   successful application of imidazolium IL in the unrolling and dispersion of MWCNT,[10] a few

8   studies have been reported about its use as a medium in the direct exfoliation of graphite into

9   graphene sheets. Wang *et al.* employed ultrasound to directly exfoliate graphite flakes in the

10   IL 1-*n*-butyl-3-methylimidazolium bis(trifluoromethanesulfonyl)imide (BMImNTf$_2$), which

11   was followed by high-speed centrifugation to remove the fast sedimenting non-exfoliated

12   graphite.[29] The supernatant IL suspension contained up to 0.95 mg/mL of graphene sheets.

13   Nuvoli *et al.* showed that a more concentrated graphene-IL suspension (5.33 mg/mL) could

14   be obtained when grinding graphite flakes and 1-*n*-hexyl-3-methylimidazolium

15   hexafluorophosphate in a mortar, before sonication.[30] The produced graphene sheets exhibited

16   an average thickness of ~ 2 nm (6-7 layers). When using the IL 1-*n*-butyl-3-

17   methylimidazolium hexafluorophosphate, Shang *et al.* exfoliated natural graphite by

18   sequential mechanical grinding and sonication into graphene sheets of 2-5 layers.[31] Another

19   approach was used by Matsumoto *et al.*, applying a polymeric IL with the

20   hexafluorophosphate anion.[32] Microwave irradiation decomposed this anion under the

21   formation of HF molecules, which intercalated within the graphite galleries and promoted

22   exfoliation.

23   Although significant progress has been achieved in the preparation of graphene, a

24   simple and high-yielding procedure for the large-scale production of cheap defect-free single-

25   or few-layer graphene with large area and smooth edges remains a challenge.[26] As this seems

26   being the main requisite to explore the full potential of graphene in the development of high-

27   tech applications,[33] this study addresses the development of a simple one-step procedure for

28   the preparation of graphene from the inexpensive untreated graphite ore. For the first time,

29   graphite ore has been completely delaminated, treating an IL containing biphasic solvent

30   system with cavitation in a pressurized ultrasonic reactor. This allowed not only obtaining

31   defect-free graphene, but also enabled the facile segregation of the graphene from the mineral

32   impurities.

1   **Experimental**

2   **Materials**

3   A crystalline graphite ore (carbon content of 48 wt.%; mined in Lazec – situated in the

4   Southbohemian Moldanubicum region) and a natural graphite powder (carbon content of

5   96 wt.% and flake diameter in the range of 3-30 μm) were kindly provided by Koh-i-noor

6   Grafite,   Ltd.,   Czech   Republic.   1-*n*-Butyl-3-methylimidazolium

7   bis(trifluoromethylsulfonyl)imide (BMImNTf$_2$; purity $\geq$ 98%) and 1-octanol (C$_8$H$_{17}$OH;

8   purity $\geq$ 99.5%) were purchased from Sigma-Aldrich. Dichloromethane (CH$_2$Cl$_2$; purity $\geq$

9   99.5%) was supplied by Lach-Ner.

10   **Graphite exfoliation in high-pressure ultrasound reactor (HP-US)**

11   Graphite ore (0.3 g), together with the biphasic water (95 mL) and organic solvent

12   (CH$_2$Cl$_2$ or C$_8$H$_{17}$OH, 5 mL) system, and IL BMImNTf$_2$ in the indicated quantity, was added

13   to an ultrasound reactor and pressurized to 5 bar (UIP 2000hd, 20 kHz, 2000 W, Hielscher

14   Ultrasonics GmbH). The reaction vessel was connected to a refrigerated recirculator, keeping

15   the reaction temperature at ~10 °C. Three different sonication programs were applied, using in

16   all cases 1.3 kW of sonication power: (i) 10 min of uninterrupted exposition, (ii) two 15 min

17   expositions intercalated with a 5 min interval (total sonication time: 30 min), and (iii) two 15

18   min and one 20 min expositions intercalated with two 5 min intervals (total sonication time:

19   50 min) (Fig. 1). Following the sonication process, the obtained suspensions were stored in

20   glass vessels.

21   **Atomic force microscopy (AFM)**

22   A Dimension Icon Atomic Force Microscope (Bruker) was used to record the AFM

23   images. A silicon tip on a nitride lever was employed for the measurement in ScanAsyst-air

24   contact mode. Two methods were used to deposit the sample on a suitable support prior the

25   measurement. (i) The majority of the samples were prepared by a spin-coating method; where

26   the samples were pipetted (20-40 μL) onto a smooth mica support and spread over the

27   substrate by rotation. (ii) The rest of the samples were prepared by depositing a drop on a

28   glass microscope slide.

29   **Transmission electron microscopy (TEM)**

1   TEM samples were deposited onto copper TEM grids (300 mesh) coated with a holey

2   carbon, washed few times with CH_2Cl_2 and imaged using a Tecnai G2 Spirit Twin at 120 kV

3   (FEI).

4   **High resolution transmission electron microscopy (HRTEM)**

5   Samples for HRTEM were first diluted in CH_2Cl_2 and put into bath ultrasound for

6   5 min. Then, the diluted sample was deposited onto carbon-coated lacey TEM grid. The

7   solvent was left to evaporate and the sample was dried under dynamic vacuum at 80°C for 4

8   hours. HRTEM and selected area electron diffraction (SAED) were carried out using a FEI

9   Talos transmission electron microscope operating at 120 kV.

10   **X-ray diffraction (XRD)**

11   Diffraction patterns of thin films on a silicon sample holder were measured using a

12   diffractometer Bruker D2 equipped with a conventional X-ray tube (CuKα radiation, 30 kV,

13   10 mA). The following conditions were used: 0.6 mm primary divergence slit module width,

14   Soler Module 2.5, 2 mm Airscatter screen module, 0.5 mm Ni Kbeta-filter, 5-90° range,

15   0.00405° steps; 0.3 s per step, and the LYNXEYE 1-dimensional detector. The crystallite

16   size, interlayer spacing and number of C atom layers were calculated using the Debye–

17   Scherrer equations.[34,35]

18   **Raman spectroscopy**

19   The Raman spectra were taken on a DXR Raman microscope (Thermo Scientific)

20   using a 10x objective lens (Olympus microscope) with a 532 nm (3 mW) laser excitation,

21   being the average of 32 two-second scans. Graphene/graphite dispersions were dropped on

22   plasma-treated microscopic glasses, 3 times washed with CH_2Cl_2 and dried at 60 °C.

23   **X-ray photoelectron spectroscopy (XPS)**

24   Thin films were prepared from CH_2Cl_2-diluted graphene/graphite dispersions on

25   plasma-treated microscopic glasses, followed by drying under vacuum at 80 °C. The XPS

26   measurements were carried out on a K-Alpha$^+$ XPS spectrometer (ThermoFisher Scientific)

27   operating at a base pressure of 1.0×10^{-7} Pa. The data acquisition and processing were

28   performed using the Thermo Avantage software. All samples were analyzed using a

29   microfocused, monochromated Al Kα X-ray radiation (400 μm spot size) with a pass energy

30   of 200 eV for survey and 50 eV for high-energy resolution core level spectra. The X-ray angle

31   of incidence was 30° and the emission angle was along the surface normal. The K-Alpha

1 charge dual compensation system was employed during analysis, using electrons and low-

2 energy argon ions to prevent any localized charge build-up. The obtained high-resolution

3 spectra were fitted/deconvoluted with Voigt profiles (binding energy uncertainty: ± 0.1 eV).

4 The analyzer transmission function, Scofield sensitivity factors, and effective attenuation

5 lengths (EAL) for photoelectrons were applied for quantification. EAL were calculated using

6 the standard TPP-2M formalism. All spectra were referenced to the C 1s peak attributed to

7 C—C, C—H at 285.0 eV binding energy, which were controlled by means of the well-known

8 photoelectron peaks of metallic Cu, Ag, and Au.

9 **Results and discussion**

10   Biphasic solvent systems, composed of organic (CH_2Cl_2 or $C_8H_{17}OH$) and water

11 phase, were used as medium for graphite ore delamination to graphene sheets in a high-

12 pressure ultrasound reactor (HP-US). At the same time, the graphite flakes were isolated from

13 the country rock due to the differences in surface tension. Contrary to the conventional

14 flotation techniques where only the mineral impurities attached to the surface of graphite

15 flakes are removed,[36] in this system the "intercalated" ash that resides between adjacent

16 graphene layers` stack is separated from the formed graphene sheets. As demonstrated in

17 Fig. 1, the purified graphene sheets were mainly trapped on water-organic solvent interphase,

18 covered the organic solvent-glass interface and partially located in the organic phase, whilst

19 the mineral impurities remained in the water phase. The use of organic solvents with different

20 densities allowed choosing where the phase with obtained graphene was *i.e.*, CH_2Cl_2 is denser

21 than water and graphene stayed from the interphase to the lower phase (Fig. 1b), while

22 $C_8H_{17}OH$ is less dense than water trapping graphene from interphase to the upper phase (Fig.

23 1c).

24
25 Fig. 1 Photographic images of the graphite ore fragment used and the dispersions obtained
26 before pressurized sonication in H_2O-CH_2Cl_2 (a) and after pressurized sonication in H_2O-

1 CH$_2$Cl$_2$ (b) and in H$_2$O-C$_8$H$_{17}$OH (c) systems. Images (b) and (c) were taken 3 months after
2 the vials were stored.

3 The influence of the particles wettability by the liquids is a first order parameter in the
4 particles adsorption behavior at the fluid-fluid interphase. When omitting any kinetic effects,
5 the preferential adsorption of the formed graphene particles on the water-organic solvent
6 interphase, in the equilibrium state, is governed by thermodynamics` tendency to minimize
7 the interfacial energy.[37] The knowledge of interfacial tensions between both liquids and
8 between liquids and graphene should be sufficient to calculate wettability parameter and to
9 predict the graphene`s location in the biphasic system. The calculated wettability parameter
10 predicts the graphene location at the interphase, which was confirmed by the experiments (the
11 details are given in the supporting information). Preferentially, high aspect ratio planar
12 graphene sheets adsorb at the liquid-liquid interphase, which has also been described in the
13 literature for water-chloroform[38] and water-heptane[39] systems. Interestingly, no sedimentation
14 and re-aggregation could be observed in the dispersions after storage for 3 months (Fig. 1),
15 indicating that the interfacial graphene layers were very stable and energetically more
16 favorable than restacking and agglomeration of the graphene sheets.[38]

17 Imidazolium IL have demonstrated huge potential as medium in the unrolling of
18 MWCNT and the exfoliation of graphite.[10] Especially, the hydrophobic IL BMImNTf$_2$
19 appears being extremely compatible with these approaches, acting not only as a surfactant for
20 carbon nanobjects through π–π stacking (graphene-imidazolium cation),[40] but also as the
21 "unrolling/exfoliating" agent when applying specific sonication conditions.[10] In the current
22 study, a similar effect of BMImNTf$_2$ was observed on the graphite ore exfoliation and
23 dispersion when applied as additive. The delamination kinetics in the absence and presence of
24 0.3 wt.% of BMImNTf$_2$ were investigated using TEM and XRD techniques (Fig. 2).

25 According to the TEM images, no graphite ore delamination was observed after 10
26 min of sonication in the absence of IL (Fig. 2a). For this case, the total sonication time had to
27 be prolonged up to 50 min (Fig. 2c) to produce graphene sheets. This exfoliation progress was
28 also observed by XRD (Fig. 2). The graphite diffraction pattern contains a typical (002)
29 reflection at $2\theta = 26.4°$, corresponding to the basal distance of 0.336 nm. Its diffraction
30 intensity (002) decreased progressively after 30 min and 50 min of pressurized sonication
31 (Fig. 2). On the other hand, the IL containing system showed a much more efficient graphite
32 delamination, as graphene sheets were already formed after 10 min of sonication (Fig. 2d).
33 The XRD diffractogram is in agreement with this observation, presenting already a drastic

1 decrease in the intensity of the (002) diffraction peak after 10 min (Fig. 2). After 30 min, the

2 (002) peak intensity was much lower compared to those measured from samples without IL,

3 confirming the beneficial role of $BMImNTf_2$ in this process.
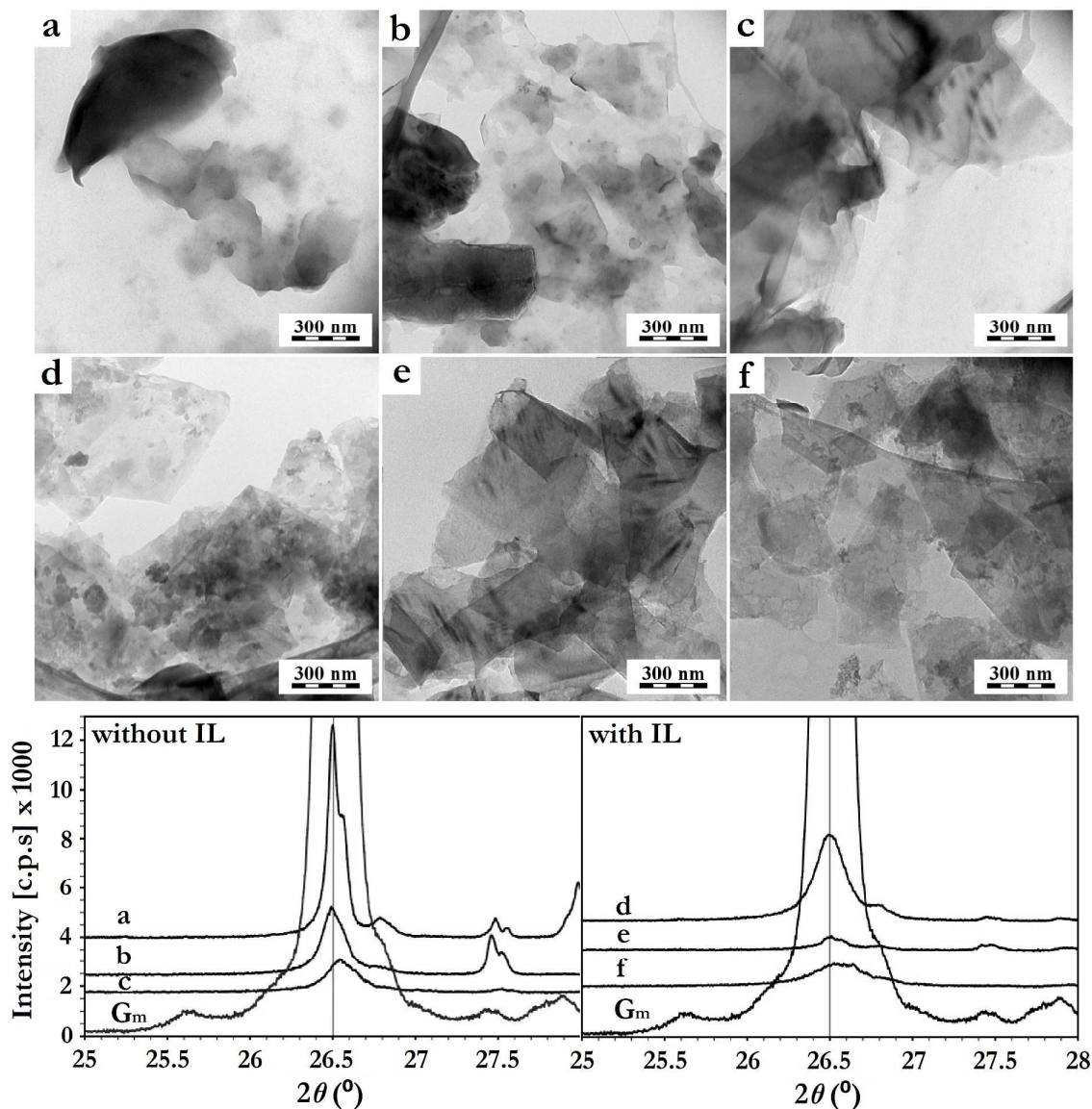
4

5 Fig. 2 TEM images and XRD diffractograms of dispersed graphite-graphene after 10 min (a),

6 30 min (b) and   50 min (c) sonication in the H_2O-CH_2Cl_2 system, and after   10 min (d),

7 30 min (e) and   50 min (f) sonication in the H_2O-CH_2Cl_2-IL system. The XRD pattern of

8 pristine graphite ore (G_m) is given for comparison.

9   In spite of the samples dilution and washing with CH_2Cl_2 prior to TEM analyses, the

10 presence of IL (aggregated gray spots) on the graphene sheets was observed. This is in

11 agreement with the strong π–π interaction between the imidazolium ring of $BMImNTf_2$ and

12 the graphene surface.[10,29,30,41] The physical adsorption of IL on the graphene sheets surface

13 was further investigated using XPS (Table 1). An increase in the nitrogen content and the

1 appearance of sulfur and fluorine indicated the $BMImNTf_2$ presence on the graphene surface.

2 Notably, the N:F:S ratio (considering the nitrogen increment due to the presence of IL) was

3 1.5:3.0:1.1 which was in excellent agreement with the expected theoretical ratio for

4 $BMImNTf_2$ (1.5:3.0:1.0). Moreover, the heteroatom-carbon proportion obtained corresponds

5 to that of the IL`s molecular composition. Considering that $BMImNTf_2$ has the molecular

6 formula $C_{10}H_{15}F_6N_3O_4S_2$, the expected C1s:O1s ratio of neat IL is 2.5. The obtained C1s:O1s

7 for exfoliated graphite without and with IL were 4.57 and 2.64, respectively. As a

8 consequence, it is reasonable to infer that most of the atomic contribution obtained by XPS

9 was from the IL, thus explaining the increased O1s values and excluding the possibility of an

10 oxidative process. The high-resolution C1s, N1s, S2p and F1s spectra of exfoliated graphite

11 ore can be found in the supporting information (Fig. S1).

12 Table 1 XPS elemental compositions of exfoliated graphite ore obtained in the absence or
13 presence of IL.

Orbital	Exfoliated graphite ore		Exfoliated graphite ore + IL	
	atomic %	weight %	atomic %	weight %
S2p	0.0	0.0	1.1 ± 0.3	6.1 ± 0.6
C1s	81.4 ± 0.3	76.7 ± 0.4	69.6 ± 1.4	63.3 ± 1.4
N1s	0.8 ± 0.1	0.9 ± 0.1	2.3 ± 0.2	2.7 ± 0.2
O1s	17.8 ± 0.3	22.4 ± 0.3	26.4 ± 2.6	25.3 ±3.0
F1s	0.0	0.0	3.0 ± 0.6	5.2 ± 0.9

14 The degree of graphite exfoliation was determined by AFM (Fig. 3). Graphene flakes

15 with an average thickness of 1-1.5 nm were obtained after pressurized sonication for 50 min

16 without IL addition (Fig. 3c and f). When IL was added, graphene flakes with a thickness of <

17 1.5 nm were produced within a much shorter sonication time of 10 min (Fig. 3a and d).

18 Additional sonication (30 min in total) led to further thickness reduction of the graphene

19 flakes to ~1.0 nm (Fig. 3b and e). Considering the thickness of single graphene layer

20 (0.335 nm),[42] 10 min and 30 min of pressurized sonication in the presence of IL led to

21 graphene flakes with less than 5 and 3 layers, respectively. As the XPS analyses confirmed

22 the presence of IL on the graphene surfaces (Table 1), their presence on the graphene sheets,

23 as well as between the mica substrate and graphene sheets, cannot be excluded. Thus, the

24 amount of graphene layers could in fact be smaller, indicating the formation of bilayers and

25 monolayers. Furthermore, Hernandez *et al.* observed on AFM images thicker graphene

26 monolayers than expected (1–2 nm instead of 0.3 nm).[19] Generally, the thicknesses ≤ 1 nm

27 determined from AFM height profiles are consistent with the formation of graphene.[43-45]

1   The AFM study provided further information about the dimensions of the obtained

2   graphenes. IL-assisted pressurized sonication produced after 10 min graphene sheets with

3   much larger lateral dimensions (average diameter of 1100 ± 350 nm) compared to those

4   obtained after 50 min in an IL-free system (average diameter of 380 ± 75 nm) (Fig. 3). This

5   reduction in the lateral dimensions could indicate transversal breakage due to a too long

6   exposition to intense cavitation.[46] The IL seems to help dissipating the excessive cavitation

7   energy, since a similar phenomenon of graphene sheets lateral size reduction was only

8   observed after 50 min of exposition, and in a much less intense manner (Fig. 2f).
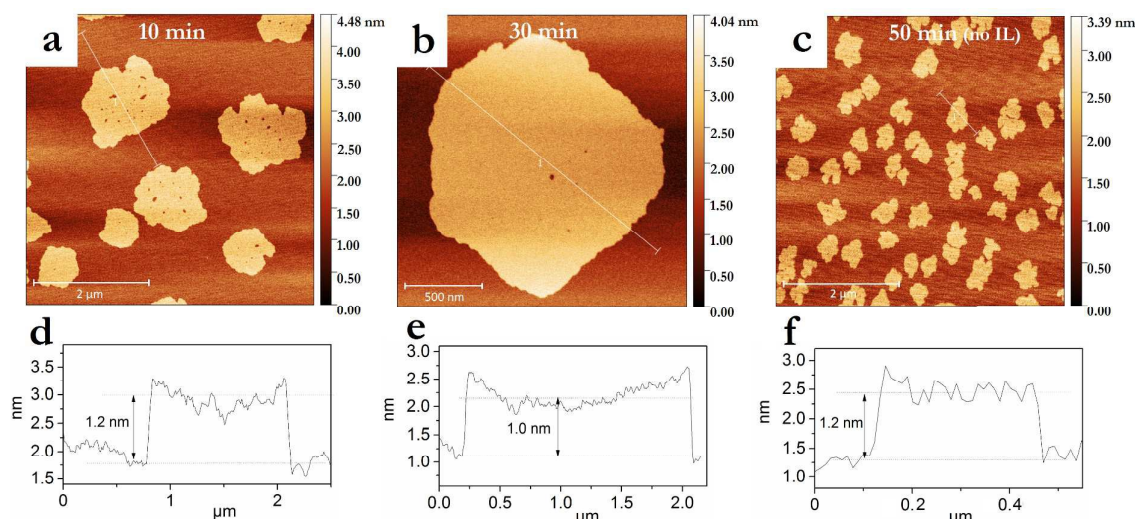
9
10   Fig. 3 AFM topology images of graphene sheets obtained after 10 min (a) and 30 min (b)
11   pressurized sonication in the H_2O-CH_2Cl_2-IL system, and (c) 50 min of pressurized sonication
12   in the H_2O-CH_2Cl_2 system. The graphs (d), (e) and (f) are the height profiles along the lines
13   displayed in (a), (b) and (c), respectively.

14   The quality of the graphene sheets produced by the best evaluated procedure (30 min

15   sonication in the presence of IL) was further evaluated by TEM (Fig. 4). Confirming the

16   previous characterizations, mostly few-layers (Fig. 4a) and monolayer (Fig. 4b) graphene

17   were formed. HRTEM (Fig. 4c) and two-dimensional fast Fourier transform (FFT) (Fig. 4d)

18   images of the formed layers showed sets of district spots at 0.21 and 0.12 nm, which

19   correspond to periodic hexagonal structure of AB Bernal stacked few-layer graphene.[47] The

20   selected-area electron diffraction pattern taken from Fig. 4b is displayed in Fig. 4e, and the

21   diffracted intensity taken along the (1–210)–(0–110)–(–1010)–(–2110) axis for this pattern is

22   displayed in Fig. 4f. The inner peaks, (0–110) and (–1010), were more intense than the outer

23   ones, (1–210) and (–2110), confirming the presence of a graphene monolayer in Fig. 4b.[19,48]

24   Besides, all observed areas seemed to be free of structural defects, evidencing that this

25   exfoliation procedure was nondestructive. In the case of the systems with IL, the sheet edges

1   also tended to bend (Fig. 3b) and crumple (Fig. 4a). Moreover, HRTEM images showed

2   regions where fringes were observed, which indicated local curvature of the sheets.[49]
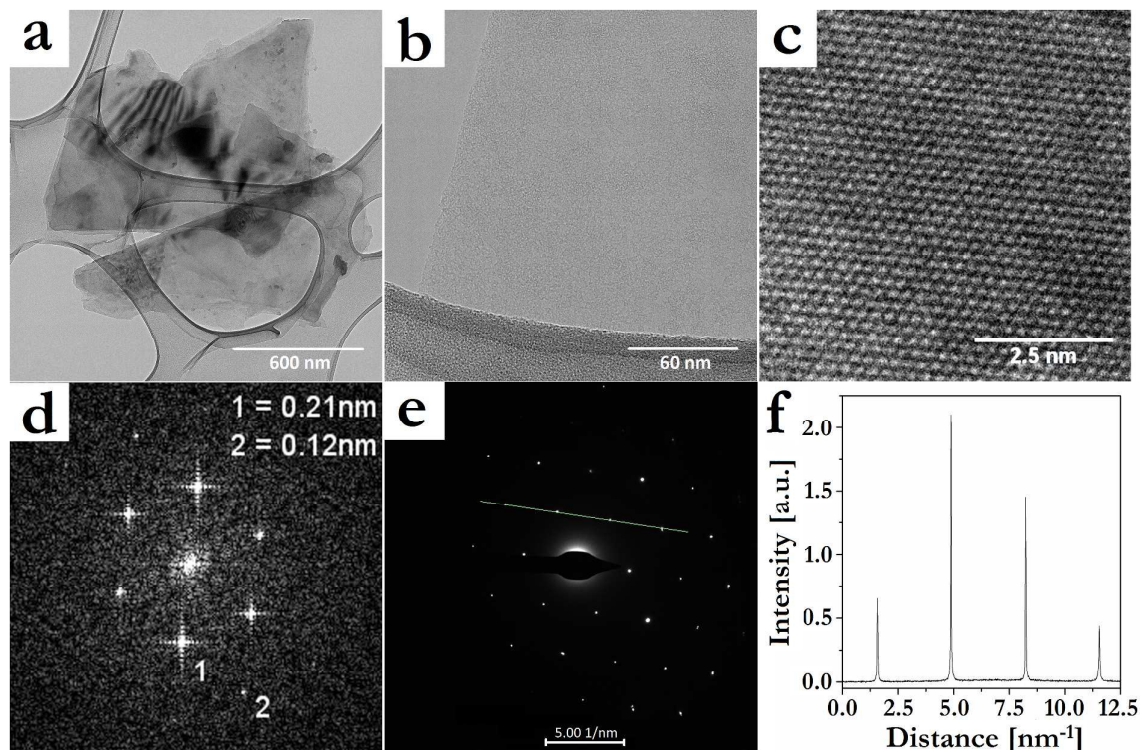
3
4   Fig. 4 Electron microscopy of graphene sheets obtained after 30 min HP-US in H_2O-CH_2Cl_2
5   in the presence of IL. TEM micrographs of (a) few-layers and (b) monolayer graphene;
6   HRTEM micrograph (c) of a few-layers graphene taken from (a); two-dimensional FFT (d) of
7   few-layers graphene taken from (a); electron diffraction patterns (e) of monolayer graphene
8   taken from (b); diffracted intensity (f) taken along the (1–210)–(0–110)–(–1010)–(–2110) axis
9   from the pattern shown in (e).

10   The exfoliating experiments were also successfully performed when the H_2O-

11   $C_8H_{17}OH$ biphasic system was used. As in the case of H_2O-CH_2Cl_2, $BMImNTf_2$ accelerated

12   the whole exfoliation process. The intensity of the XRD 002 peak ($2\theta = 26.5$) decreased to

13   less than 1% of its initial value after 30 minutes of pressurized sonication, indicating

14   structural disordering and graphite exfoliation,[32] in a slightly lower degree when compared to

15   the H_2O-CH_2Cl_2 system (Fig. S2). HRTEM images confirmed the formation of few-layers

16   thick graphene sheets (Fig. S3).

17   Raman spectroscopy is another important tool to determine the graphene quality.

18   Fig. S4 shows the Raman spectra of bulk graphite ore and cast films from the graphene

19   suspensions (without and with $BMImNTf_2$). Graphitic materials typically involve three bands;

20   (i) the D-band (~ 1350 cm^{-1}), (ii) the G-band (~ 1580 cm^{-1}) and (iii) the 2D-band (~ 2700 cm^{-1}

21   $^{-1}$).[50] The D/G band intensity ratio (I_D/I_G) is often used for determining the graphene`s degree

1   of structural defects.[51] Thus, a smaller I_D/I_G ratio means a lower number of defects and

2   disorders in the graphitic structure, comprising the disorders caused at the edges of the

3   platelets;[52] therefore, the D-band intensity is influenced by the flake size.[26,53] All prepared

4   graphene films showed I_D/I_G ratio identical to the one of the pristine graphite ore (ca. 0.15,

5   Table S2), confirming the high structural integrity of the produced graphene sheets.[32]

6   Commercial powdered natural graphite, extracted from the graphite ore by a

7   conventional treatment, was also applied in the developed method and used as a comparison

8   to the direct graphite ore exfoliation. The same pressurized sonication time (30 min) was

9   sufficient to completely delaminate the powdered natural graphite in the biphasic H_2O-

10   CH_2Cl_2 system containing 0.3 wt.% of BMImNTf$_2$. The XRD pattern (Fig. S2), TEM images

11   and SAED (Fig. S5) gave evidence that few-layers and monolayer graphene sheets were also

12   formed. The similar graphene sheets obtained, for both graphite ore and commercial

13   powdered graphite, evidence the effectiveness of the process and highlight the advantages of a

14   direct processing of the graphite ore.

15   Most interestingly, when a higher amount of CH_2Cl_2 (50 v.%) was added to the

16   process a different behavior was observed after 30 min of sonication. Macroporous swelled

17   species with micrometric lateral dimension were formed in high yield (Fig. 5a). These seem to

18   be constituted by few layers of crumpled graphene, forming two main types of structure; (i)

19   large macroporous segments (Fig. 5b), and (ii) pine cone-like structures[54] formed by few

20   layers of entangled and crumpled graphene (Fig. 5c). These structures were probably created

21   due to the more intensive intercalation of IL-CH_2Cl_2 in between graphite galleries. As this

22   phenomenon occurred exclusively with the IL-CH_2Cl_2 system, it seems to be a synergistic

23   solvent-coupling agent effect. In Fig. 5d and e, AFM evidenced the formation of a graphene

24   bilayer (~ 1 nm thick) with swollen central regions (2-3 nm thick), indicating that the swelling

25   could be due to cavitation induced bubble formation from the intercalated IL-CH_2Cl_2. The

26   two different structures formed could be a result of different local sheet size and chemical

27   composition. The phase transition between a flat-membrane phase and the crumpled phase

28   has been reported to have a notable dependence on the size, functionalization and defects of

29   the graphene sheets.[55] Thus; the predominant presence of layered crumpled graphene

30   structures was also an indication of the small content of sheet defects.
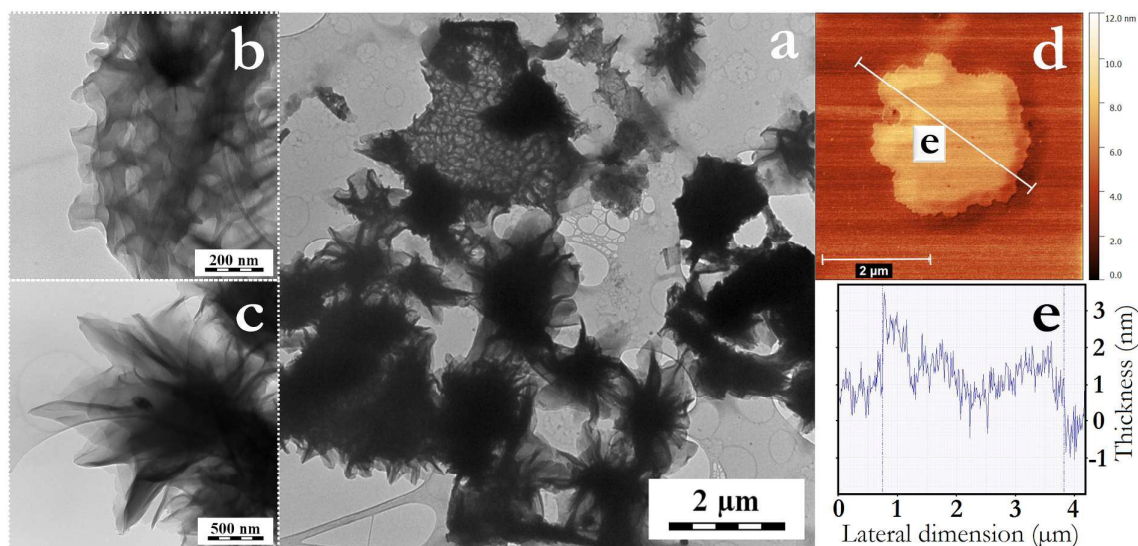
Fig. 5 Microscopic images of the crumpled graphene-graphite species formed by biphasic pressurized sonication procedure at higher CH_2Cl_2 content; TEM image the general morphological aspect (a) and higher magnification of the "macroporous" (b) and "pine cone-like" (c) species formed. AFM topological image (d) and height profile (e) of a swelled graphene bilayer.

Conclusions

The pressurized sonication of a biphasic system represents a cheap and effective method for the exfoliation of graphite ore into few-layers graphene. This reaction set-up avoids the need of a centrifugation purification procedure, as the mineral impurities originated from the graphite ore are collected in the water phase or settle down at the bottom, whilst the produced graphene sheets are located at the liquid-liquid interface and in the organic phase. The addition of IL ($BMImNTf_2$) considerably reduced the exfoliation time and produced graphene sheets with much larger lateral dimensions. Although preliminary, also a prospective, simple and straightforward method for the controlled production of crumpled graphene materials has been demonstrated. Since these processes produce graphene sheets with non-covalently bonded $BMImNTf_2$ on the surface, the modified graphene species could be used in a vast range of materials applications without altering the pristine graphene characteristics. The system optimization and the role of different ionic liquids into the final materials` morphology are an active subject of our group and will be explored in details in further publications.

Acknowledgement

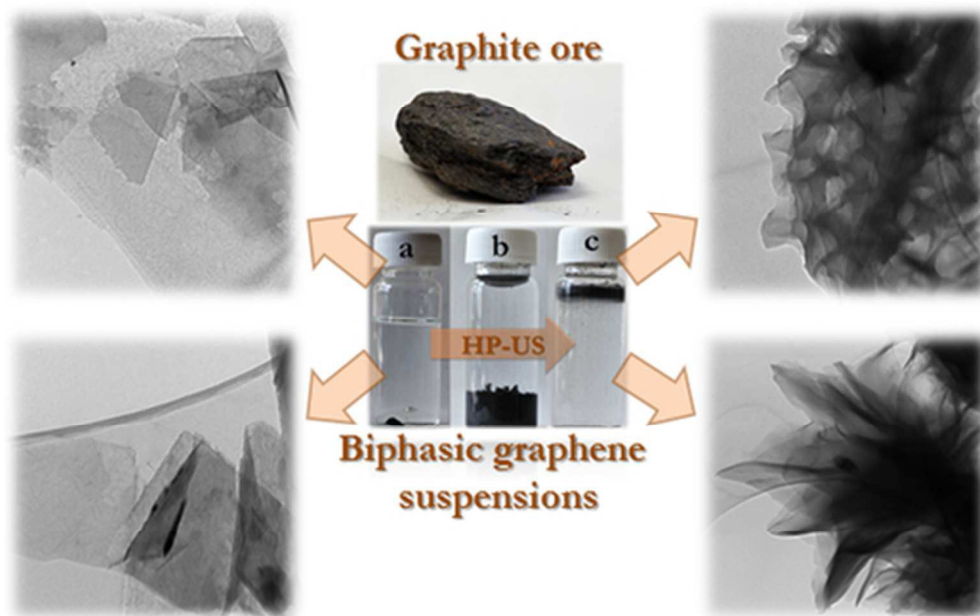## References

1. M. Terrones, A. R. Botello-Mendez, J. Campos-Delgado, F. Lopez-Urias, Y. I. Vega-Cantu, F. J. Rodriguez-Macias, A. L. Elias, E. Munoz-Sandoval, A. G. Cano-Marquez, J. C. Charlier and H. Terrones, *Nano Today*, 2010, **5**, 351.

2. A. K. Geim, *Science*, 2009, **324**, 1530.

3. A. K. Geim and K. S. Novoselov, *Nat. Mater.*, 2007, **6**, 183.

4. K. S. Novoselov, A. K. Geim, S. V. Morozov, D. Jiang, Y. Zhang, S. V. Dubonos, I. V. Grigorieva and A. A. Firsov, *Science*, 2004, **306**, 666.

5. X. Zhang, A. C. Coleman, N. Katsonis, W. R. Browne, B. J. van Wees and B. L. Feringa, *Chem. Commun.*, 2010, **46**, 7539.

6. S. Stankovich, D. A. Dikin, R. D. Piner, K. A. Kohlhaas, A. Kleinhammes, Y. Jia, Y. Wu, S. T. Nguyen and R. S. Ruoff, *Carbon*, 2007, **45**, 1558.

7. O. C. Compton and S. B. T. Nguyen, *Small*, 2010, **6**, 711.

8. X. Qi, K.-Y. Pu, X. Zhou, H. Li, B. Liu, F. Boey, W. Huang and H. Zhang, *Small*, 2010, **6**, 663.

9. S. Vadahanambi, J.-H. Jung, R. Kumar, H.-J. Kim and I.-K. Oh, *Carbon*, 2013, **53**, 391.

10. A. C. Kleinschmidt, R. K. Donato, M. Perchacz, H. Benes, V. Stengl, S. C. Amico and H. S. Schrekker, *RSC Adv.*, 2014, **4**, 43436.

11. Q. Liu, T. Fujigaya, N. Nakashima, *Carbon*, 2012, **50**, 5421.

12. K. V. Emtsev, A. Bostwick, K. Horn, J. Jobst, G. L. Kellogg, L. Ley, J. L. McChesney, T. Ohta, S. A. Reshanov, J. Rohrl, E. Rotenberg, A. K. Schmid, D. Waldmann, H. B. Weber and T. Seyller, *Nat. Mater.*, 2009, **8**, 203.

13. X. Li, W. Cai, J. An, S. Kim, J. Nah, D. Yang, R. Piner, A. Velamakanni, I. Jung, E. Tutuc, S. K. Banerjee, L. Colombo and R. S. Ruoff, *Science*, 2009, **324**, 1312.

14. J.-W. Lee, M. Kim, W. Na, S. M. Hong and C. M. Koo, *Carbon*, 2015, **91**, 527.

15. A. Dato, V. Radmilovic, Z. Lee, J. Phillips and M. Frenklach, *Nano Lett.*, 2008, **8**, 2012.

16. S. Guo, S. Dong, *Chem. Soc. Rev.*, 2011, **40**, 2644.

17. C. N. R. Rao, A. K. Sood, K. S. Subrahmanyam and A. Govindaraj, *Angew. Chem. Int. Ed.*, 2009, **48**, 7752.

18. V. Stengl, *Chem. Eur. J.*, 2012, **18**, 14047.

19. Y. Hernandez, V. Nicolosi, M. Lotya, F. M. Blighe, Z. Y. Sun, S. De, I. T. McGovern, B. Holland, M. Byrne, Y. K. Gun'ko, J. J. Boland, P. Niraj, G. Duesberg, S. Krishnamurthy, R. Goodhue, J. Hutchison, V. Scardaci, A. C. Ferrari and J. N. Coleman, *Nat. Nanotechnol.* 2008, **3**, 563.

20. W. F. Zhao, M. Fang, F. R. Wu, H. Wu, L. W. Wang and G. H. Chen, *J. Mater. Chem.*, 2010, **20**, 5817.

21. Z. Wei, D. E. Barlow and P. E. Sheehan, *Nano Lett.*, 2008, **8**, 3141.

22. Z. Osvath, A. Darabont, P. Nemes-Incze, E. Horvath, Z. E. Horvath and L. P. Biro, *Carbon*, 2007, **45**, 3022.

23. E. K. Choi, I. Y. Jeon, S. Y. Bae, H. J. Lee, H. S. Shin, L. M. Dai and J. B. Baek, *Chem. Commun.*, 2010, **46**, 6320.

24. M. Lotya, Y. Hernandez, P. J. King, R. J. Smith, V. Nicolosi, L. S. Karlsson, F. M. Blighe, S. De, Z. Wang, I. T. McGovern, G. S. Duesberg and J. N. Coleman, *J. Am. Chem. Soc.*, 2009, **131**, 3611.

25. R. Peng, Y. Wang, W. Tang, Y. Yang and X. Xie, *Polymers*, 2013, **5**, 847.

26. J. N. Coleman, *Acc. Chem. Res.*, 2013, **46**, 14.

27. S. Wang, Y. Zhang, N. Abidi and L. Cabrales, *Langmuir*, 2009, **25**, 11078.

28. S. Bellayer, J. W. Gilman, N. Eidelman, S. Bourbigot, X. Flambard, D. M. Fox, H. C. de Long and P. C. Trulove, *Adv. Funct. Mater.*, 2005, **15**, 910.

29. X. Q. Wang, P. F. Fulvio, G. A. Baker, G. M. Veith, R. R. Unocic, S. M. Mahurin, M. F. Chi and S. Dai, *Chem. Commun.*, 2010, **46**, 4487.

30. D. Nuvoli, L. Valentini, V. Alzari, S. Scognamillo, S. B. Bon, M. Piccinini, J. Illescas and A. Mariani, *J. Mater. Chem.*, 2011, **21**, 3428.

31. N. G. Shang, P. Papakonstantinou, S. Sharma, G. Lubarsky, M. Li, D. W. McNeill, A. J. Quinn, W. Zhou and R. Blackley, *Chem. Commun.*, 2012, **48**, 1877.

32. M. Matsumoto, Y. Saito, C. Park, T. Fukushima and T. Aida, *Nature Chem.*, 2015, **7**, 730.

33. M. Peplow, *Nature*, 2015, **522**, 268.

34. B. Sakintuna, Y. Yurum and S. Cetinkaya, *Energy Fuels*, 2004, **18**, 883.

35. B. Saner, F. Okyay and Y. Yurum, *Fuel*, 2010, **89**, 1903.

36. http://asbury.com/technical-presentations-papers/materials-in-depth/natural-flake-graphite/

37. F. Fenouillot, P. Cassagnau and J. C. Majeste, *Polymer*, 2009, **50**, 1333.

38. S. Biswas and L. T. Drzal, *Nano Letters*, 2008, **9**, 167.

39. S. J. Woltornist, A. J. Oyer, J. M. Y. Carrillo, A. V. Dobrynin and D. H. Adamson, *ACS nano*, 2003, **7**, 7062.

40. T. Fukushima and T. Aida, *Chem. Eur. J.*, 2007, **13**, 5048.

41. X. Zhou, T. Wu, K. Ding, B. Hu, M. Hou and B. Han, *Chem. Commun.*, 2010, **46**, 386.

42. B. T. Kelly, *Physics of Graphite*, Applied Science: London, 1981.

43. A. B. Bourlinos, V. Georgakilas, R. Zboril, T. A. Steriotis and A. K. Stubos, *Small*, 2009, **5**, 1841.

44. P. Nemes-Incze, Z. Osváth, K. Kamaras and L. P. Biro, *Carbon*, 2008, **46**, 1435.

45. I. Jung, D. A. Dikin, R. D. Piner and R. Ruoff, *Nano Letters*, 2008, **8**, 4283.

46. M. Yi and Z. Shen, *J. Mater. Chem. A*, 2015, **3**, 11700.

47. J. H. Warner, M. H. Rummeli, L. Ge, T. Gemming, B. Montanari, N. M. Harrison, B. Buchner, G. A. D. Briggs, *Nat. Nanotechnol.*, 2009, **4**, 500.

48. V. Stengl, J. Henych, J. Bludska, P. Ecorchard, and M. Kormunda, *Ultrasonics sonochemistry*, 2015, **24**, 65.

49. S. Stankovich, D. A. Dikin, G. H. B Dommett, K. M. Kohlhaas, E. J. Zimney, E. A. Stach, R. D. Piner, S. T. Nguyen and R. S. Ruoff, *Nature*, 2006, **442**, 282.

50. R. Satio, M. Hofmann, G. Dresselhaus, A. Jorio and M.S. Dresselhaus, *Adv. Phys.*, 2011, **60**, 413.

51. M. M. Lucchese, F. Stavale, E. M. Ferreira, C. Vilani, M.. V. O. Moutinho, R. B. Capaz, C. A. Achete and A. Jorio, *Carbon*, 2010, **48**, 1592.

52. O. Akhavan, *ASC Nano*, 2010, **4**, 4174.

53. U. Khan, A. O'Neill, M. Lotya, S. De and J. N. Coleman, *Small*, 2010, **6**, 864.

54. Y. Zhao, J. Feng, X. Liu, F. Wang, L. Wang, C. Shi, L. Huang, X. Feng, X. Chen, L. Xu, M. Yan, Q. Zhang, X. Bai, H. Wu and L. Mai, *Nat. Comm.*, 2014, **5**, 4565.

55. C. Chang, Z. Song, J. Lin and Z. Xu, *RSC Adv.*, 2013, **3**, 2720.

44x28mm (300 x 300 DPI)